Mechanism of the Bisphosphatase Reaction of 6-Phosphofructo-2-kinase/Fructose-2,6-Bisphosphatase Probed by ^{1}H-^{15}N NMR Spectroscopy†

David A. Okar, David H. Live, Matthew H. Devany, and Alex J. Lange*

University of Minnesota, Medical School and College of Biological Sciences, Department of Biochemistry, Molecular Biology, and Biophysics, 321 Church Street S.E., Minneapolis, Minnesota 55455

Received April 11, 2000; Revised Manuscript Received June 2, 2000

ABSTRACT: The histidines in the bisphosphatase domain of rat liver 6-phosphofructo-2-kinase/fructose-2,6-bisphosphatase were labeled with ^{15}N, both specifically at N1′ and globally, for use in heteronuclear single quantum correlation (HSQC) NMR spectroscopic analyses. The histidine-associated ^{15}N resonances were assigned by correlation to the C2′ protons which had been assigned previously [Okar et al., *Biochemistry 38*, 1999, 4471−79]. Acquisition of the ^{1}H-^{15}N HSQC from a phosphate-free sample demonstrated that the existence of His-258 in the rare N1′ tautomeric state is dependent upon occupation of the phosphate binding site filled by the O2 phosphate of the substrate, fructose-2,6-bisphosphate, and subsequently, the phosphohistidine intermediate. The phosphohistidine intermediate is characterized by two hydrogen bonds involving the catalytic histidines, His-258 and His-392, which are directly observed at the N1′ positions of the imidazole rings. The N1′ of phospho-His-258 is protonated (^{1}H chemical shift, 14.0 ppm) and hydrogen bonded to the backbone carbonyl of Gly-259. The N1′ of cationic His-392 is hydrogen bonded (^{1}H chemical shift, 13.5 ppm) to the phosphoryl moiety of the phosphohistidine. The existence of a protonated phospho-His-258 intermediate and the observation of a fairly strong hydrogen bond to the same phosphohistidine implies that hydrolysis of the covalent intermediate proceeds without any requirement for an "activated" water. Using the labeled histidines as probes of the catalytic site mutation of Glu-327 to alanine revealed that, in addition to its function as the proton donor to fructose-6-phosphate during formation of the transient phosphohistidine intermediate at the N3′ of His-258, this residue has a significant role in maintaining the structural integrity of the catalytic site. The ^{1}H-^{15}N HSQC data also provide clear evidence that despite being a surface residue, His-446 has a very acidic pK_a, much less than 6.0. On the basis of these observations a revised mechanism for fructose-2,6-bisphosphatase that is consistent with all of the previously published kinetic data and X-ray crystal structures is proposed. The revised mechanism accounts for the structural and kinetic consequences produced by mutation of the catalytic histidines and Glu-327. It also provides the basis for a hypothetical mechanism of bisphosphatase activation by cAMP-dependent phosphorylation of Ser-32, which is located in the N-terminal kinase domain.

Fructose-2,6-bisphosphate[1] is an allosteric activator of 6-PF-1-K and an allosteric inhibitor of F-1,6-BPase, therefore, it is a primary determinant of carbohydrate flux in liver (*1*). The bifunctional enzyme, 6-PF-2-K/F-2,6-BPase, plays a major role in the control of hepatic gluconeogenic/glycolytic fluxes because it is the sole enzyme responsible for both the synthesis and degradation of F-2,6-P_2 and thereby modulates the intracellular concentration of this signal metabolite (*2*, *3*). The kinase and bisphosphatase reactions take place at two distinct sites within the 55 kDa rat liver enzyme with the kinase domain in the N-terminal region and the bisphosphatase domain in the C-terminal region (*4*). The concentration of F-2,6-P_2 is determined by the relative activities of these domains, defined as the K/BP ratio, which is dependent upon the phosphorylation state of Ser-32 (*5*). Phosphorylated bifunctional enzyme has a low K/BP and functions to reduce F-2,6-P_2 levels, while dephosphorylated enzyme has a high K/BP and serves to increase F-2,6-P_2 levels. The cAMP-dependent phosphorylation of Ser-32 is mediated by glucagon, while glucose promotes dephosphorylation via a xyulose-5-phosphate-dependent protein phosphatase (*5*, *6*). Therefore, the opposing actions of glucose and glucagon on hepatic carbohydrate flux can be understood, at least in part, by their modulation of the K/BP of the bifunctional enzyme. These observations provide the impetus for the detailed study of the bisphosphatase reaction because inhibition of the hepatic bisphosphatase would raise the

† This work was supported by NIH Grant RO1-DK38354 to A.J.L. and ADA Research Award to D.A.O..

* To whom correspondence should be addressed: E-mail: lange024@tc.umn.edu. Phone: (612) 626-4502. Fax: (612) 625-5476.

[1] Abbreviations: F-2,6-P_2, fructose-2,6-bisphosphate; F-6-P, fructose-6-phosphate; 6-PF-1-K, 6-phosphofructo-1-kinase; F-1,6-BPase, fructose-1,6-bisphosphatase; 6-PF-2-K/F-2,6-BPase, 6-phosphofructo-2-kinase/fructose-2,6-bisphosphatase; K/BP, kinase-to-bisphosphatase activity ratio; ul, universally labeled; HSQC, heteronuclear single quantum correlation; His-P, phosphohistidine; ND249.WT, wild-type rat liver bisphosphatase domain derived from N-terminal deletion of 249 amino acids from the bifunctional enzyme. Point mutants are indicated by including the residue number and mutation, i.e., ND249.H446A means that His-446 has been mutated to alanine, The numbering of all amino acids refers to the rat liver enzyme, except where specified. The imidazole ring of histidine is numbered according to the common biochemical scheme: N1′ = $N^{\delta 1}$, C2′ = $C^{\epsilon 1}$, N3′ = $N^{\epsilon 2}$, C4′ = $C^{\delta 2}$, and C5′ = Cγ.

10.1021/bi000815k CCC: $19.00
Published on Web 07/14/2000

F-2,6-P_2 level and direct carbohydrate flux toward glycolysis, thus lowering hepatic glucose production. This would lower blood glucose levels and relieve the hyperglycemia associated with the diabetic state (*7*).

The separately expressed rat liver bisphosphatase domains are devoid of kinase activity, yet, possess steady-state bisphosphatase activity very similar to the dephosphorylated bifunctional enzyme (*8*, *9*). The bisphosphatase hydrolyzes F-2,6-P_2 to F-6-P and P_i via a covalent N3′ phosphohistidine intermediate at His-258 by an ordered, sequential mechanism (*10*−*12*). The active site contains the signature RHG motif at Arg-257, His-258, and Gly-259, as well as, Arg-307, Glu-327, and His-392 (*13*, *14*). Putative roles for each of these amino acid residues in catalysis have been assigned by site-directed mutagenesis and steady-state kinetic analyses (*13*−*15*). The X-ray crystal structures of the resting enzyme and the phosphohistidine intermediate complex confirmed that these residues are located in the active site (*16*−*18*). The ^{31}P NMR studies demonstrated that the E-P:F-6-P complex is predominant during turn-over and confirmed that dissociation of the F-6-P from the phosphohistidine intermediate is the rate-limiting step in the bisphosphatase reaction (*12*). In our previous NMR study, the histidine C2′-associated ^{13}C and ^{1}H resonances assigned to His-258, His-392, His-419, and His-446 did not titrate over the pH range 5.5−10.0, indicating that these residues maintain their protonation and tautomeric states over this range (*19*).

We have used ^{15}N labeling, both specifically at the N1′ of histidine and globally, to confirm the predicted protonation and tautomeric states of the histidines and to probe the reaction mechanism. The extreme stability of the transient phosphohistidine intermediate allowed a detailed comparison of the wild-type and mutant bisphosphatases during turnover. The ability to acquire NMR spectra of the reaction intermediate combined with the sensitivity of histidine-associated ^{15}N chemical shifts to the chemical environment, i.e., hydrogen bonding, and the availability of X-ray structures has provided sufficient data to relieve most of the ambiguities concerning the reaction mechanism of the bisphosphatase. We present a mechanism for the wild-type enzyme that is consistent with all published kinetic, structural, and NMR data. This mechanism, along with the ^{15}N NMR data acquired from mutants of His-258 and Glu-327, can fully account for their reduced bisphosphatase activity. Furthermore, it provides insight as to how the regulatory phosphorylation at the distant Ser-32 site can result in activation of the bisphosphatase.

EXPERIMENTAL PROCEDURES

Protein Expression and Purification. The rat liver bisphosphatase domain was produced by expression in the BL21(DE3) and the BL21(DE3) his− auxotroph produced in our laboratory from the pET3a vector (Novagen, Madison, WI) as described previously (*20*). Globally ^{15}N-labeled proteins were produced by including 98% [^{15}N]$(NH_4)_2SO_4$ (Cambridge Isotope Laboratories, Andover, MA) as the sole nitrogen source in the M10 media developed in our laboratory (*20*). Bisphosphatase specifically labeled with ^{15}N at the N1′ was prepared by addition of 99% [^{15}N]N1′ histidine (Cambridge Isotope Laboratories, Andover, MA) to cultures of the BL21(DE3) his− strain harboring the pET3a vector encoding the protein of interest. The construction of all pET3a vectors encoding for the alanine point mutants of ND249 have been reported elsewhere (*14*, *19*). Purification was accomplished as previously described (*19*). All samples were judged to be greater than 95% pure by SDS/PAGE analysis.

Sample Preparation. After purification all samples were dialyzed into 100 mM sodium phosphate, pH 8.0 and concentrated by ultrafiltration through YM10 membranes (Amicon, Beverly, MA). The samples were exchanged into 100 mM sodium phosphate, pH 7.0, by repeated dilution and concentration in the ultrafiltration device. A phosphate-free sample of ND249.WT was made in 50 mM tris, pH 7.0, 300 mM KCl by the same method. The NMR samples were prepared in either 10 or 90% D_2O depending upon the spectra that were to be acquired. All samples were dialyzed against the same buffer prior to data acquisition. Sample pH was monitored just prior to acquisition of the NMR data and, if any additions were made to the sample, afterward also. The pH values agreed to within 0.2 units in all cases. Samples were between 0.9 and 2.9 mM as determined by the BCA protein assay (Pierce, Rockford, IL).

NMR Spectroscopy. ^{1}H-^{15}N gradient HSQC experiments employing a sensitivity enhancement scheme were collected on a Varian Unity INOVA 600 MHz spectrometer with a 5 mm gradient HCN triple resonance probe (*21*). The ^{1}H spectral width was 15 000 Hz with an acquisition time of 68 μs, and the ^{15}N spectral width was 12 400 Hz with 64 increments in the indirectly detected dimension. The interval in the HSQC transfer was tuned to 95 or 28 Hz depending on whether one bond, $^{1}J_{NH}$, or two bond, $^{2}J_{HN}$, correlations were being observed. This is similar to the methods employed by Pelton et al. in which the HSQC experiment was optimized to account for the effects of spin relaxation by adjusting the interval to reveal the maximum number of cross-peaks (*22*). The pertinent coupling constants for the histidine ring were taken from Blomberg et al. (*23*). A relaxation delay of 1 s was inserted before each scan. Data were processed using the Varian VNMR software, zero filled to 2048 points in the ^{1}H dimension and 512 points in the ^{15}N dimension. The known position of the water resonance was used to calibrate the proton chemical shift scale which was used in turn to calculate the ^{15}N shifts (*24*).

RESULTS

Resonance Assignments. The histidine-associated ^{15}N resonances were assigned in the wild-type enzyme by a series of ^{1}H-^{15}N HSQC spectra acquired from ND249.WT and the mutants, ND249.H258A and ND249.H258A.H392A, all specifically labeled at the N1′ of histidine. The $^{2}J_{HN}$ spectrum of wild-type enzyme presented in Figure 1 A correlates the previously assigned C2′ ^{1}H resonances (*19*) with the ^{15}N shifts from the N1′ position for His-304, His-344, His-446, and His-469 via the two-bond scalar coupling. Resonances for the three remaining histidine residues were not detected in this experiment, presumably because their C2′ protons relax rapidly and magnetization could not be efficiently transferred to the nitrogens. This explanation is consistent with the broad resonances observed for His-258, His-392, and His-419 in the previous study (*19*). Three cross-peaks were detected in the $^{1}J_{NH}$ spectrum of the specifically labeled

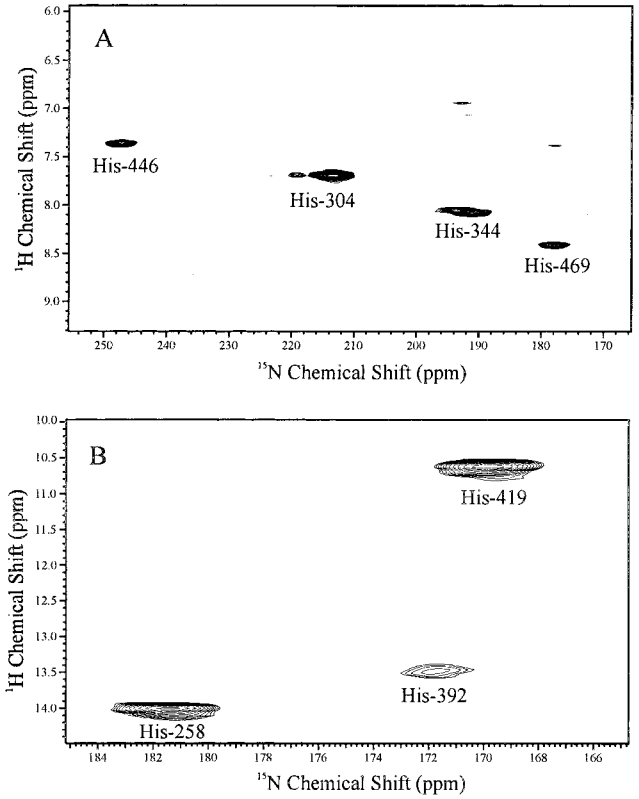

FIGURE 1: HSQC spectra of ND249.WT specifically labeled with ^{15}N at the N1′ of histidine. (A) The $^2J_{HN}$ region that correlates the ^{1}H resonance of the C2′ position with the ^{15}N resonance of the N1′ position via 2-bond coupling. Sample was prepared in 90% D_2O. (B) The $^1J_{NH}$ region that correlates the ^{1}H resonance with the ^{15}N resonance of the N1′ position via 1-bond coupling. Sample was prepared in 10% D_2O. Spectra were acquired as stated in the Experimental Procedures, and both samples were in 100 mM sodium phosphate, pH 7.0 at 25 °C.

protein, shown in Figure 1B, that reveal the protons directly bound to the N1′ of the histidine rings. Because the ^{15}N chemical shift for each of the cross-peaks in the spectrum given in Figure 1B is unique, i.e., does not match any detected in the $^2J_{HN}$ spectrum in Figure 1 A, the data in Figure 1 account for all seven histidine residues in ND249.WT. Assignment of the His-258, His-392, and His-419 cross-peaks in Figure 1B were accomplished by acquisition of $^1J_{NH}$ HSQC spectra for the pertinent alanine point mutants (data not shown).

When the same spectra were acquired from ul-^{15}N ND249.WT the HSQC data were identical to those acquired from the specifically labeled material for cross-peaks in the $^1J_{NH}$ region. Figure 2 shows the $^2J_{HN}$ region for the globally labeled sample where signals from the N3′ nitrogens and C4′ protons for some histidines were detected. The chemical shifts were assigned based upon the spectra in Figure 1 and the patterns predicted by Pelton et al. (*22*). The determination of both ^{15}N shifts in a given histidine ring is definitive for the tautomeric and protonation states (*22*, *25*). The resonance assignments for the histidines of ND249.WT are compiled in Table 1.

Mutational Analyses. The replacement of Glu-327 with alanine caused a structural rearrangement of the catalytic site that is revealed by the comparison of the ^{1}H-^{15}N spectra acquired from mutant enzyme globally labeled with ^{15}N, Figure 3, with those of the wild-type, Figures 1 and 2. In

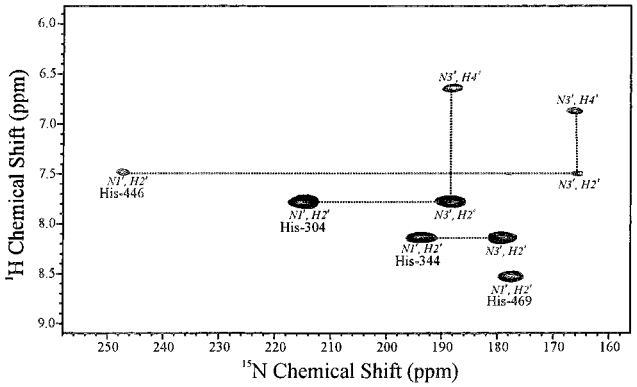

FIGURE 2: $^2J_{HN}$ region of an HSQC spectrum acquired from ND249.WT globally labeled with ^{15}N. The $^1J_{NH}$ region is not shown because it is identical to that seen with the N1′ specifically labeled samples (Figure 1B). Sample was prepared in 90% D_2O and 100 mM sodium phosphate, pH 7.0 at 25 °C. Acquisition parameters were as stated in the Experimental Procedures.

Table 1: Histidine Ring Chemical Shifts in Wild-Type Fructose-2,6-bisphosphatase Domain in 100 mM Sodium Phosphate, pH 7.0 at 25 °C

	^{15}N (ppm)		^{13}C (ppm)	^{1}H (ppm)		
histidine	N1′	N3′	C2′[a]	C2′[a]	N1′	C4′
258	181.8	nd[b]	138.4	9.89	13.9	nd
304	213.4	188.0	138.0	7.75	nd	6.65
344	191.3	179.5	137.3	8.00	nd	nd
392	171.2	nd	137.3	7.14	13.3	nd
419	169.2	nd	137.3	7.25	10.5	nd
446	247.2	165.8	139.2	7.47	nd	6.85
469	178.0	nd	136.9	8.50	nd	7.44

[a] Taken from ref *19*. [b] nd, not detected.

the $^2J_{HN}$ region of the spectrum, the E327A mutant has cross-peaks that were not observed in the same type of spectrum acquired from wild-type bisphosphatase. These were assigned to His-258 and His-419 by comparison of the C2′ proton chemical shifts to those determined for the same mutant in the ^{1}H-^{13}C HSQC study (*19*). The single cross-peak observed in the $^1J_{NH}$ spectrum of ND249.E327A was assigned to His-392 by the process of elimination. These assignments were confirmed by the HSQC spectra acquired from the ND249.H258A, ND249.H258A.E327A, and ND249.H258A.H392A mutants specifically labeled at the N1′ of histidine. These chemical shifts are given in Table 2. Perturbations of the histidine-associated ^{15}N and ^{1}H resonances due to the point mutations were localized to the catalytic site (His-258 and His-392) and the nearby His-419. This observation confirms that the structural changes incurred by these mutations are site-specific and are not due to large-scale unfolding or alterations of the global structure. The replacement of the phosphoacceptor, His-258, with alanine specifically perturbed the resonances of His-392 and, to a lesser extent, those of His-419. Among all of the mutations studied herein, the ND249.E327A mutation imparts the greatest perturbations of the catalytic site, furthermore, these perturbations are relieved in the double mutant (ND249.H258A.E327A).

Transient Phosphohistidine Intermediate. When a 10× molar excess of F-2,6-P_2 was added to either ND249.WT or ND249.E327A the resulting 1-bond correlation spectra are almost identical, as shown in Figure 4. The three cross-peaks

Table 2: Chemical Shifts for His-258, His-392, and His-419 in Various Point Mutants of the Catalytic Residues Determined in 100 mM Sodium Phosphate, pH 7.0 at 25 °C

	His-258 (ppm)				His-392 (ppm)			His-419 (ppm)		
	C2′	N1′	N1′	N3′	C2′	N1′	N1′	C2′	N1′	N1′
mutation	^{1}H[a]	^{1}H	^{15}N	^{15}N	^{1}H[a]	^{1}H	^{15}N	^{1}H[a]	^{1}H	^{15}N
E327A	8.31	nd	200.0	175.6	7.65	12.96	171.9	7.28	nd[c]	179.5[b]
H258A					7.40	10.80	168.0	7.22	10.52	168.0
H258A.E327A					7.18	14.55	168.0	7.26	10.56	168.0
H258A.H392A								7.23	10.32	168.5

[a] Taken from previous ^{1}H-^{13}C HSQC spectra (*19*). [b] Detected in the $^2J_{HN}$ region of the HSQC spectrum. [c] nd, not detected.

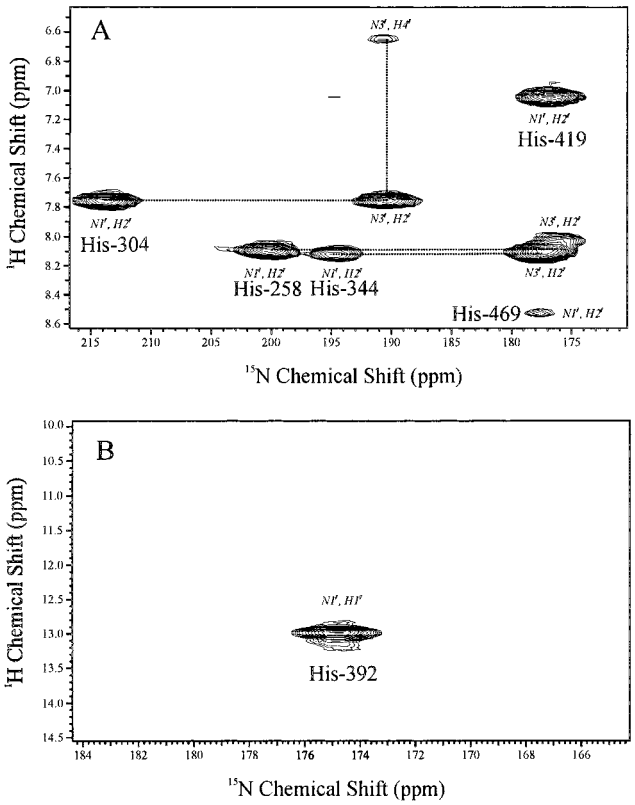

FIGURE 3: HSQC spectra of ND249.E327A globally labeled with ^{15}N. (A) The $^2J_{HN}$ region that correlates the ^{1}H resonance of the C2′ position with the ^{15}N resonance of the N1′ position via 2-bond coupling. Sample was prepared in 90% D_2O. B) The $^1J_{NH}$ region that correlates the ^{1}H resonance with the ^{15}N resonance of the N1′ position via 1-bond coupling. Sample was prepared in 10% D_2O. Spectra were acquired as stated in the Experimental Procedures and both samples were in 100 mM sodium phosphate, pH 7.0 at 25 °C.

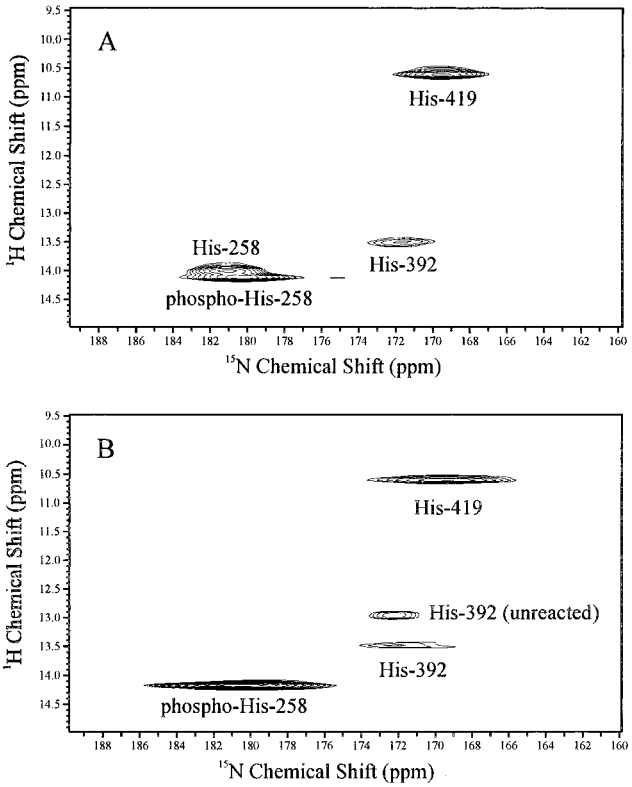

FIGURE 4: $^1J_{NH}$ region of the HSQC spectra acquired from bisphosphatase in the transient phosphohistidine intermediate complex. All cross-peaks in this region are correlations at the N1′ position of the histidine rings. (A) ND249.WT and (B) ND249.E327A. Both samples were prepared in 10% D_2O and were globally labeled with ^{15}N. Spectra were acquired as stated in the Experimental Procedures and both samples were in 100 mM sodium phosphate, pH 7.0 at 25 °C.

that are related to the transient phosphohistidine intermediate, His-419, His-392, and phospho-His-258, are detected at the same chemical shifts in HSQC spectra both the wild-type and the mutant bisphosphatases. The remaining cross-peaks, 14.00 ppm ^{1}H/181.2 ppm ^{15}N in Figure 4A and 12.95 ppm ^{1}H/172.0 ppm ^{15}N in Figure 4B arise from bisphosphatase that is unreacted, i.e., not in the transient intermediate complex, and reflect the chemical shifts of His-258 in the wild-type and His-392 in the mutant resting enzymes, respectively. These data indicate that the resting state conformations of His-392 and His-258 are different in the E327A mutant and wild-type enzymes, but very similar in the transient intermediate complex. This means that after the phosphohistidine has been formed the microstructure of the catalytic site is not perturbed by the E327A mutation. The 2-bond correlation region of the HSQC spectra acquired from wild-type and ND249.E327A in the transient intermediate were consistent with this assertion (data not shown).

However, because the 1- and 2- bond HSQC spectra are acquired from H_2O and D_2O samples, respectively, the ^{15}N1′ resonance of His-419 was shifted downfield by approximately 1.5 ppm in H_2O relative to that in D_2O. To determine whether this shift could be fully explained by the deuterium exchange we determined the solvent dependence of the ^{15}N chemical shifts in histidine by titrating free histidine with pH in H_2O and D_2O (data not shown). On this basis, we concluded that a deuterium isotope effect at the N1′ of protonated histidine shifts the ^{15}N resonance downfield by approximately 1.5 ppm.

DISCUSSION

Protonation and Tautomeric States of the Histidines in the Bisphosphatase. Table 3 lists the protonation and

Table 3: Protonation and Tautomeric States of the Histidines in Rat Liver Bisphosphatase Domain in 100 mM Sodium Phosphate, pH 7.0[a]

histidine	ND249.WT (resting enzyme)	ND249.E327A (resting enzyme)	transient intermediate (wild-type and mutant)
258	neutral N1′	neutral N3′	cationic[b]
304	neutral N3′	neutral N3′	neutral N3′
344	neutral N3′	neutral N3′	neutral N3′
392	cationic	cationic	cationic
419	cationic	cationic	cationic
446	neutral N3′	neutral N3′	neutral N3′
469	cationic	cationic	cationic

[a] The tautomeric state of a histidine is a property that applies only to the neutral imidazole ring and is designated by identifying which ring nitrogen, N1′ or N3′, carries the proton. This is distinct from the cationic imidazolium ion in which both ring nitrogens are protonated, or the anionic imidazolate ion in which the ring is completely deprotonated. [b] The His-258 is phosphorylated at the N3′ and protonated at the N1′ in the transient intermediate which produces a cationic imidazole ring.

tautomeric state of each histidine in the wild-type and E327A mutant, as well as in the transient phosphohistidine intermediate. The ^{15}N chemical shifts determined for the histidines in the wild-type bisphosphatase domain confirm that His-392, His-419, and His-469 are protonated in the wild-type bisphosphatase domain and of the remaining histidines only His-258 can exist in the N1′ tautomeric form. These results are completely consistent with the protonation and tautomeric states that were predicted on the basis of the C2′ ^{13}C and ^{1}H chemical shifts (*19*). Because the seven histidines in the bisphosphatase exist in a broad spectrum of protonation states they provide an ideal system to demonstrate the utility of the method developed by Pelton et al. to predict the patterns detected in ^{1}H-^{15}N correlation spectra of histidine (*22*). The HSQC spectrum in Figure 2 shows that His-446 gives a clear spectral signature for a neutral N3′ tautomer of histidine. The ^{15}N chemical shifts perfectly match those predicted by Pelton et al. The ^{1}H chemical shifts, however, show much less dispersion than predicted, 6.65−7.44 ppm (experimental) versus 5.80−8.30 (predicted).

The N1′ ^{15}N resonances of the 3 histidines that were titrated by pH in our previous report (*19*), His-304, His-344, and His-469 appear progressively upfield from that of His-446. This is just as expected from the predicted spectra and the fact that these residues exist in mixed protonation states due to their pK_as and the neutral pH at which the ^{1}H-^{15}N HSQC data were acquired. The observation that each of these histidines gave rise to a single set of cross-peaks implies that the protonation/deprotonation exchange rate is fast relative to the NMR time-scale. The further upfield the N1′ ^{15}N resonance, the more protonated the given residue because in the fast exchange regime the resonances appear at an average position weighted by the relative amount of each state. On this basis, we conclude that His-446 has a pK_a that is even more acidic than that of His-304, which was determined to be less than 6.0 by pH titration of the C2′ ^{13}C and ^{1}H resonances (*19*). In fact, the pK_a of His-446 may be even lower than 4.5 because chemical shifts of its C2′ ^{13}C and ^{1}H resonances were not altered during the pH titration over the range 4.5−9.0 (*19*). The observation of a surface histidine residue with such a strongly perturbed pK_a is intriguing and may be related to the putative role of His-446 in linking the C-terminal region to the catalytic site, as will be discussed below.

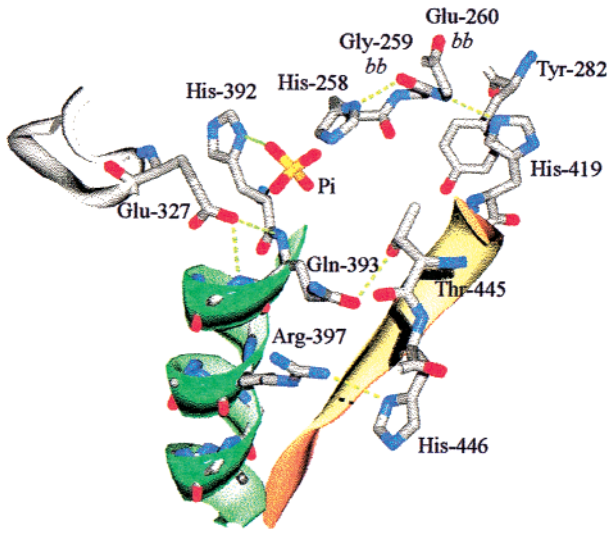

FIGURE 5: View of the bisphosphatase catalytic site derived from the molecular coordinates of the rat testes bifunctional enzyme, 1BIF, the truncated rat liver bisphosphatase domain, 1FBT, and the NMR data (*16*, *18*). For clarity, some of the secondary structural elements and hydrogen bonding interactions described in the text are not shown. The *bb* designation for Gly-259 and Glu-260 indicates that only the *b*ack-*b*one atoms are shown for these residues, not the side chains. Note that Tyr-282 in the rat liver enzyme is equivalent to Phe-280 in the rat testes isoform. The figure was prepared with the Swiss PDB Viewer 3.51 (Glaxo-Wellcome) and POV-Ray 3.1 (Indianapolis, IN).

The observation of intense cross-peaks in the $^{1}J_{NH}$ region for His-258, His-392, and His-419 (Figure 1B) indicates that these protons are involved in significant hydrogen bonding within the bisphosphatase or are sequestered from interaction with solvent because under normal circumstances the imidazole NH protons exchange rapidly with solvent and are not observed (*26*). The cross-peaks for these imidazole NH are not detected in D_2O, which suggests that these histidines are accessible to solvent. The cross-peak at 14.00 ppm ^{1}H/181.2 ppm ^{15}N in the HSQC spectrum of ND249.WT is definitive evidence that His-258 is protonated at the N1′ position. The downfield proton chemical shift is indicative of fairly strong hydrogen bonding and this may account for the observation that the ^{15}N resonance is further downfield than that predicted for an N1′ tautomer (*27*). The situation is similar for His-392 and His-419, the relatively deshielded proton chemical shifts indicate that these residues are hydrogen bond donors at the N1′ position. The existence of these hydrogen bonds accounts for the observed resistance of these histidine residues to pH titration (*19*).

Structure of the Bisphosphatase Catalytic Site and the Role of Glu-327. Some structural features of the bisphosphatase that are essential to the interpretation of the ^{1}H-^{15}N NMR data have been derived from the X-ray crystal structures of the rat testes 6-PF-2-K/F-2,6-BPase (*18*) and the C-terminal truncated rat liver bisphosphatase domain (*16*, *17*) and these are shown in Figure 5. His-392 is located at the junction between a β strand and an α helix. The helix extends from residue 393 to 405 in the rat liver bisphosphatase domain and Cys-391 is the last residue in the short stretch of β strand (*16*). This helix, along with His-392 and Cys-391 will be

referred to as the His-392 subdomain for the purposes of this discussion. Cys-391 links the His-392 subdomain to the His-258 region via a hydrogen bond to Cys-256, although for clarity this interaction is not shown in Figure 5. The His-392 subdomain is structurally conserved in the rat testes enzyme, as is the Cys-391/Cys-256 pair (*18*). His-419 is located at the end of a β strand (residues 419−427) that is antiparallel to the β strand adjacent to His-258 (residues 252−258). The N3′ of the protonated His-419 side chain is hydrogen bonded to the Nα of Glu-260 and the N1′ to the backbone carbonyl of Val- 440. His-419 is parallel to Tyr-282 and these residues are less than 5 D apart. A similar motif was observed in the rat testes enzyme for the analogous His-417 and Phe-280. Some of these interactions, specifically the hydrogen bonds to His-419, are not depicted in Figure 5 because they are not essential to bisphosphatase function. They are included in this discussion only to explain how the resonances assigned to His-419 were perturbed by the same mutations that effect the catalytic site. The association of His-419 with a parallel aromatic ring, along with the hydrogen bonds to the imidazole, explains why this residue does not titrate with pH and is characterized by a broad ^{1}H resonance at the C2′ position (*19*). His-258 is located at the C-terminal end of a short β strand, as mentioned above, although this β strand is not shown in Figure 5 for clarity. The N1′ of His-258 is hydrogen bonded to the backbone carbonyl of Gly-259, as long as the adjacent phosphate binding site is occupied. Glu-327 does not interact directly with His-258, His-392, or His-419. Interaction between Glu-327 and these residues is mediated by the His-392 subdomain, with which the carboxylate of Glu-327 has multiple hydrogen bond interactions. A bound phosphate appears in every crystal structure examined, except that of the E-P:F-6-P complex where it is replaced by the phosphohistidine, and is likely to be present in the NMR samples as well because 100 mM sodium phosphate is the primary buffer used for the NMR studies. When an ^{1}H-^{15}N HSQC spectrum was acquired from a phosphate-free sample of ul-^{15}N ND249.WT the cross-peak assigned to the N1′ imide of His-258 was eliminated and those of His-392 and His-419 were shifted (data not shown). This implies that the N1′ tautomeric state of His-258 is dependent upon occupancy of the phosphate site, while the protonation states of His-392 and His-419 are not. The ^{1}H chemical shifts of the N1′ in the phosphate-free spectrum were 12.37 and 12.51 ppm for His-392 and His-419, respectively. Because the chemical shift of a proton involved in a hydrogen bond is roughly proportional to the strength of the hydrogen bond, these data suggest that the hydrogen bond to His-419 is strengthened and that to His-392 is weakened by the removal of phosphate from the active site (*28*). The N1′ of His-419 is hydrogen bonded to the backbone NH of Glu-260 and, with phosphate present, the N1′ of His-258 is hydrogen bonded to the backbone carbonyl of Gly-259. Therefore, the hydrogen bond partners of these two histidines are separated by a single peptide bond. The disappearance of the N1′ NH cross-peak assigned to His-258 from the phosphate-free spectrum implies that the N1′ tautomeric structure is lost, which may result in a stronger hydrogen bond to His-419.

With these aspects of the bisphosphatase structure in mind, we can explain how the mutation of Glu-327 to alanine strongly perturbs the resonances of His-258 and His-419, while those of His-392 are not significantly changed. These results are qualitatively similar to those of our earlier study with ^{13}C-labeled histidine (*19*), but the greater sensitivity of the ^{15}N chemical shifts to the chemical environment provides a clearer picture of the nature of these perturbations at each histidine. The cross-peak pattern observed for His-258 in the ND249.E327A mutant (Figure 3) indicate that this mutation promotes a change in the tautomeric state of the phosphoacceptor to the N3′ species. Comparison to the cross-peak patterns for His-304 and His-344 suggest that, in the ND249.E327A mutant, His-258 has a pK_a slightly lower than that of His-344, which was determined to be 7.04 (*19*). In addition to promoting a change in the His-258 tautomeric state, the E327A mutation also allows this histidine to be detected in the $^2J_{HN}$ experiment. The latter observation, along with the narrower C2′ ^{1}H resonances observed for His-258 in the E327A mutant in the earlier work, implies that the phosphoacceptor adopts a different conformation in this mutant. However, the change in the tautomeric state of His-258 is not sufficient to cause all of the structural perturbations seen in the E327A mutant because removal of the phosphate ion appears to promote the tautomeric change, but does not alter the status of His-419 or His-392 to the same extent as mutation of Glu-327. Therefore, we conclude that the alterations of the structure of the catalytic site seen in the E327A mutant result, at least in part, from the disruption of the hydrogen bond interactions of the Glu-327 carboxylate with the His-392 subdomain.

The HSQC spectra of two other mutants also pertain to the structural role of Glu-327. The ND249.H258A mutation caused little or no perturbation of any other histidine. This implies that His-258, despite its central role in the bisphosphatase reaction, it not essential to the structural integrity of the catalytic site. Interestingly, the same mutation in the ND249.H258A.E327A enzyme reverses most of the structural perturbations produced by the E327A mutation because the ^{1}H-^{15}N HSQC spectrum of this double mutant shows much less perturbation than the E327A mutant, especially at His-419. However, the reversal of these structural changes in ND249.H258A.E327A indicates that the N3′ tautomer of His-258 has a role in the structural perturbations detected in the E327A mutant. The exact nature of these changes in the catalytic site structure cannot be fully elucidated because no structures of the E327A mutant are available.

Revised Mechanism for the Bisphosphatase. Since the first crystal structure of a bisphosphatase domain and the accompanying mechanism were published by Lee et al. a number of alternative mechanisms have been proposed (*16*, *17*, *29*, *30*). All of the mechanisms are consistent in that the reaction proceeds in two stages, formation and hydrolysis of the phosphohistidine intermediate. However, they differ widely concerning the identity of the proton donor to the F-6-P during His-P formation and how hydrolysis of the His-P is initiated. Both Glu-327 and His-392 have been identified as the proton donor group and, likewise, as the residue responsible for "activating" a bound water molecule to promote phosphohistidine hydrolysis (*29*, *30*). On the basis of the structural features revealed by our ^{1}H-^{15}N NMR analyses of the histidines of the bisphosphatase domain we have developed the revised kinetic mechanism shown in Figure 6 that is consistent with all the published data,

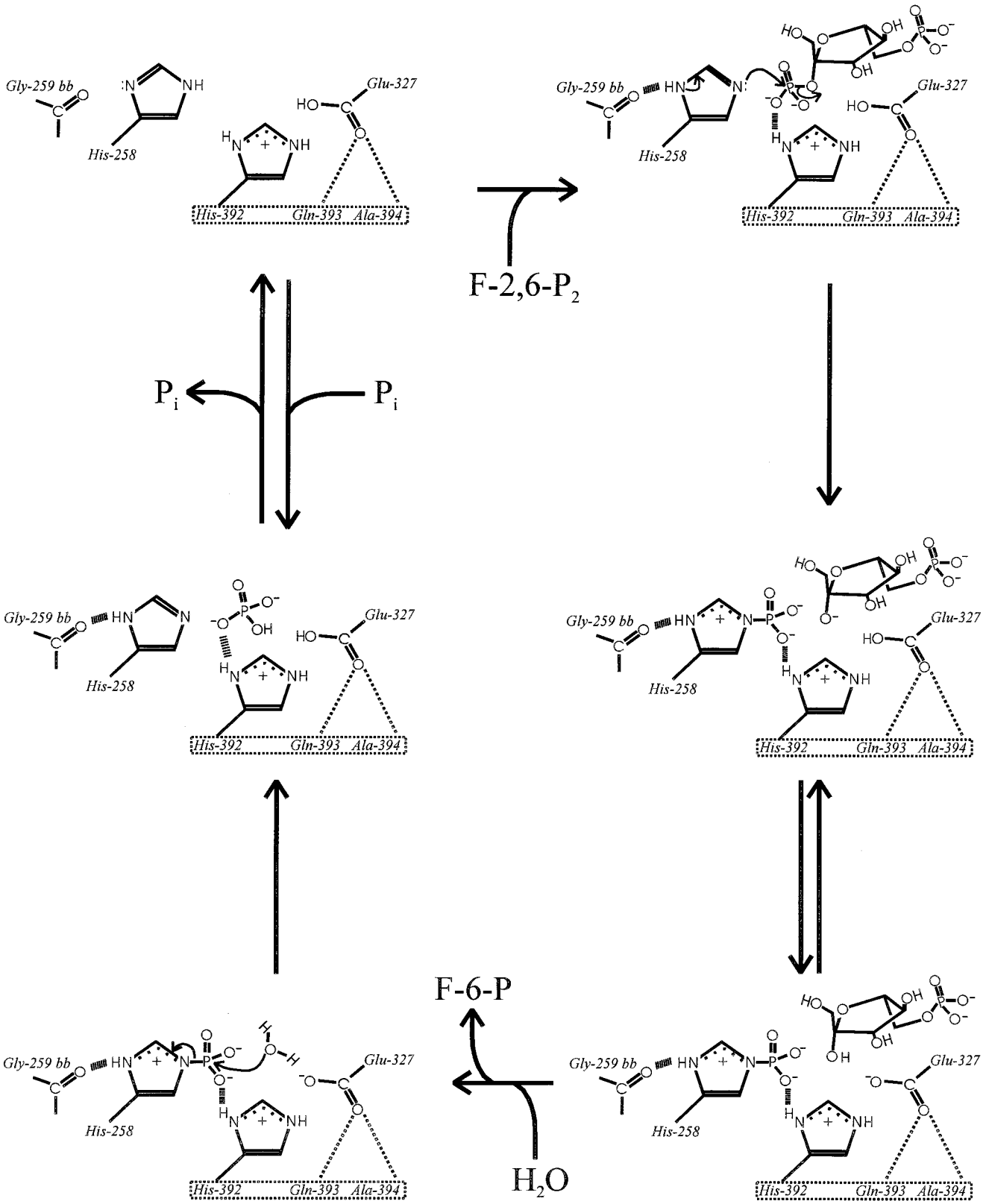

FIGURE 6: Revised mechanism of fructose-2,6-bisphosphatase. For clarity, the arginine residues, Arg-257 and Arg-307, that also coordinate to the phosphohistidine are not shown. (|||) Hydrogen bond detected by NMR; (···) hydrogen bond predicted from the X-ray structure.

including kinetic analyses of point mutants of the catalytic residues.

Starting with the resting enzyme at the upper right-hand corner of Figure 6, the reaction begins with the binding of F-2,6-P_2 into the catalytic site. This promotes the formation of the N1′ tautomer of His-258 which is stabilized by a hydrogen bond to the backbone carbonyl of Gly-259. The formation of this hydrogen bond increases the nucleophilic character of the N3′ and it attacks the C2 phosphoester of the substrate to generate the phosphohistidine. Subsequently, the O2 of the F-6-P leaving group is protonated by Glu-327. We conclude that formation of the His-P precedes

protonation of the F-6-P leaving group because kinetic data indicate that phosphohistidine formation proceeds 2 orders of magnitude faster than release of P_i (*31*). Furthermore, the phosphohistidine is fully formed prior to the protonation of the F-6-P because, as Stewart et al. suggest, it is the dissociation of *nascent* F-6-P that is the rate-limiting step of the reaction (*32*). The nascent F-6-P cannot dissociate until it is protonated at the O2 position. The phosphohistidine intermediate is characterized by at least two strong hydrogen bonds to the catalytic histidines, one between the N1′ of His-258 and the backbone carbonyl of Gly-259 and another between the N1′ of His-392 and the phosphoryl group of the phosphohistidine. Because both of these histidine rings are cationic they can effectively neutralize the excess negative charge of the phosphate oxygen atoms and make the phosphate more electrophilic. Although they are not depicted in Figure 6, Arg-257 and Arg-307 may provide the same function; neutralizing the negative charges at the phosphate oxygens. These roles have been suggested by kinetic and mutational analyses and are the focus of our ongoing NMR analyses (*14*). Certainly, the more negative charge on the phosphohistidine that is neutralized by hydrogen bonding, the more attractive the phosphate becomes to nucleophilic attack by water to complete the reaction. The kinetic and mutational study of the rat testes enzyme by Mizuguchi et al. clearly demonstrated that His-392 is involved in hydrolysis of the phosphohistidine because in the equivalent H390A[2] mutant, F-6-P dissociation precedes the release of P_i, whereas, these two are coincident in the wild-type and H256A mutants (*29*). This observation suggests that the strong hydrogen bond detected between His-392 and the phosphohistidine is essential for E-P hydrolysis. This view is confirmed by the NMR data because we have detected a strong hydrogen bond to the N1′ of a cationic His-392 which is apparently strengthened in the transient intermediate based on the downfield shift of the proton resonance. These observations imply that the role of His-392 in phosphohistidine hydrolysis is direct, and it does not activate a water molecule as suggested by Mizuguchi et al. (*29*). In fact, the revised mechanism presented here is notable because it does not require any activation of the water molecule that attacks the phosphohistidine to complete the hydrolysis because phospho-His-258 is maintained in the protonated state by the hydrogen bond to the backbone carbonyl of Gly-259, while His-392 and the arginines can sufficiently neutralize the excess negative charge. This mechanism for His-P hydrolysis can be understood by analogy to that of phosphohistidine in acid, where protonation of the imidazole ring makes the histidine a good leaving group and the resultant metaphosphate reacts quickly with water, without need of any agent to "activate" the water molecule (*33*).

The revised mechanism and the ^1H-^{15}N NMR data for the bisphosphatase can also account for the observed kinetic consequences produced by mutation of the catalytic residues (*13*). Mutation of Glu-327 to alanine, glutamine, or aspartate decreased the rate of phosphohistidine formation to approximately the same extent relative to wild-type, yet the rate of phosphohistidine hydrolysis was some 30−60 times faster in E327D than in the other two mutants. The similarity of the rate of phosphohistidine formation for the three mutants studied by Lin et al. suggests that the reason for this decrease in rate is similar for all of these mutants, despite the variety of side chains involved. This observation is consistent with a structural role for Glu-327 that only the carboxylate of glutamate can fulfill. We suggest that the slow phosphohistidine formation in these mutants is related to the disruption of the hydrogen bond interactions with the His-392 subdomain, which must then rearrange in order to form E-P. This view is strongly supported by the NMR data herein (see Figure 4) and our previous ^1H-^{13}C analyses, which clearly demonstrate that the structural changes caused by mutation of Glu-327 in the resting enzyme are reversed upon formation of the transient intermediate complex (*19*). The E327D mutant is the only one that can fulfill the role of proton donor to the F-6-P, although not as efficiently as the glutamate. This is revealed as a decreased rate of E-P hydrolysis because the phosphohistidine cannot be hydrolyzed until the F-6-P dissociates from the E-P and the F-6-P cannot dissociate until it is protonated.

Mutant bisphosphatases that lack the phosphoacceptor can still hydrolyze F-2,6-P_2 by another mechanism that does not require a covalent intermediate (*29*). Our NMR data indicate that the H258A mutation does not promote any structural rearrangement of the catalytic site, thus, all of the remaining enzymatic machinery is in place to promote the hydrolysis of substrate. Mizuguchi et al. also report that the H256A.H390A[2] double mutant of the rat testes bifunctional enzyme has the lowest bisphosphatase activity of any mutants examined, including H256A.E325A. These observations are consistent with the revised mechanism because binding the substrate into the catalytic site with concurrent formation of a strong hydrogen bond between His-392 and the C2 phosphoryl group, may neutralize enough of the charge on the phosphate to promote direct hydrolysis, much like that seen for the nonenzymatic hydrolysis of F-2,6-P_2 in acid.

Activation of the Bisphosphatase by Posttranslational Modification—A Hypothesis. Interestingly, the structural role of Glu-327 involves hydrogen bond interactions with the His-392 subdomain, the same region of the bisphosphatase that has been shown to provide a link between the catalytic site and the C-terminal regulatory domain via a hydrogen bond between Arg-397 and His-446 (see Figure 5) (*19*). Considering that protonation of the F-6-P may very well be the rate-limiting step of the reaction, i.e., the F-6-P cannot dissociate until it is protonated, the current studies allow us to hypothesize that the activation of the bisphosphatase by cAMP-dependent phosphorylation of Ser-32 involves a conformational change in the C-terminal region that is communicated to the catalytic site by the His-446 → Arg-397 linkage. This promotes a concerted movement of the His-392 subdomain which alters the position of Glu-327 in such a way as to increase the rate of F-6-P protonation and thereby activate the bisphosphatase. It is still not clear how the phosphorylation at Ser-32 can result in a conformational change in the C-terminal region, especially in light of the observation by Hasemann et al. that the crystal structure of the rat testes bifunctional enzyme shows no interaction of the bisphosphatase domains across the dimer interface (*18*).

[2] The amino acid sequence in the bisphosphatase domain of the rat testes isoform can be aligned to that of the rat liver isoform by adding 2 to the sequence number, i.e., His-256 in the rat testes is equivalent to His-258 in the rat liver enzyme.

It may be that cAMP-dependent phosphorylation changes the quaternary structure of the enzyme to allow intersubunit contacts and these, in turn, are responsible for promoting the conformational changes that result in higher bisphosphatase activity. However, this issue may only be resolved when a structure for the Ser-32 phosphorylated bifunctional enzyme becomes available.

ACKNOWLEDGMENT

NMR instrumentation was provided by the Structural Biology NMR Resource and the University of Minnesota Medical School. The authors are grateful to Dr. H. P. C. Hogenkamp at the University of Minnesota for his insightful discussions concerning the reaction mechanism.

REFERENCES

1. Pilkis, S. J., El-Maghrabi, M. R., and Claus, T. H. (1988) *Annu. Rev. Biochem. 57*, 755−83.
2. Pilkis, S. J., Claus, T. H., Kurland, I. J., and Lange, A. J. (1995) *Annu. Rev. Biochem. 64*, 799−835.
3. Argaud, D., Lange, A. J., Becker, T. C., Okar, D. A., El-Maghrabi, M. R., Newgard, C. B., and Pilkis, S. J. (1995) *J. Biol. Chem. 270*, 24229−36.
4. Lively, M. O., El-Maghrabi, M. R., Pilkis, J., D'Angelo, G., Colosia, A. D., Ciavola, J. A., Fraser, B. A., and Pilkis, S. J. (1988) *J. Biol. Chem. 263*, 839−49.
5. El-Maghrabi, M. R., Fox, E., Pilkis, J., and Pilkis, S. J. (1982) *Biochem. Biophys. Res. Commun. 106*, 794−802.
6. Nishimura, M., Fedorov, S., and Uyeda, K. (1994) *J. Biol. Chem. 269*, 26100−6.
7. Okar, D. A., Lee, Y.-H., Argaud, D., McFarlan, S. C., and Lange, A. J. (1998) in *Frontiers in Diabetes* (Belfiore, F., Ed.) S. Karger AG, Basel.
8. Tauler, A., Rosenberg, A. H., Colosia, A., Studier, F. W., and Pilkis, S. J. (1988) *Proc. Natl. Acad. Sci. U.S.A. 85*, 6642−6.
9. Lee, Y. H., Okar, D., Lin, K., and Pilkis, S. J. (1994) *J. Biol. Chem. 269*, 11002−10.
10. Pilkis, S. J., Walderhaug, M., Murray, K., Beth, A., Venkataramu, S. D., Pilkis, J., and El-Maghrabi, M. R. (1983) *J. Biol. Chem. 258*, 6135−41.
11. Stewart, H. B., El-Maghrabi, M. R., and Pilkis, S. J. (1985) *J. Biol. Chem. 260*, 12935−41.
12. Okar, D. A., Kakalis, L. T., Narula, S. S., Armitage, I. M., and Pilkis, S. J. (1995) *Biochem. J. 308*, 189−95.
13. Lin, K., Li, L., Correia, J. J., and Pilkis, S. J. (1992) *J. Biol. Chem. 267*, 6556−62.
14. Lin, K., Li, L., Correia, J. J., and Pilkis, S. J. (1992) *J. Biol. Chem. 267*, 19163−71.
15. Tauler, A., Lin, K., and Pilkis, S. J. (1990) *J. Biol. Chem. 265*, 15617−22.
16. Lee, Y. H., Ogata, C., Pflugrath, J. W., Levitt, D. G., Sarma, R., Banaszak, L. J., and Pilkis, S. J. (1996) *Biochemistry 35*, 6010−9.
17. Lee, Y.-H., Olson, T. W., Ogata, C. M., Levitt, D. G., Banaszak, L. J., and Lange, A. J. (1997) *Nat. Struct. Biol. 4*, 615−8.
18. Hasemann, C. A., Istvan, E. S., Uyeda, K., and Deisenhofer, J. (1996) *Structure 4*, 1017−29.
19. Okar, D. A., Live, D. H., Kirby, T. L., Karschnia, E. J., vonWaymarn, L. B., Armitage, I. M., and Lange, A. J. (1999) *Biochemistry 38*, 4471−9.
20. Okar, D. A., Felicia, N. D., Gui, L., and Lange, A. J. (1997) *Protein Expression Purif. 11*, 79−84.
21. Kay, L. E., Keifer, P., and Saarinen, T. (1992) *J. Am. Chem. Soc. 114*, 10663−5.
22. Pelton, J. G., Torchia, D. A., Meadow, N. D., and Roseman, S. (1993) *Protein Sci. 2*, 543−558.
23. Blomberg, F., Maurer, W., and Ruterjans, H. (1976) *Proc. Natl. Acad. Sci. U.S.A. 73*, 1409−13.
24. Wishart, D. S., Bigam, C. G., Yao, J., Abildgaard, F., and Dyson, H. J. (1995) *J. Biomol. NMR 6*, 135−140.
25. Van Dijk, A. A., Scheek, R. M., Dijkstra, K., Wolters, G. K., and Robillard, G. T. (1992) *Biochemistry 31*, 9063−9072.
26. Wuthrich, K. (1986) *NMR of Proteins and Nucleic Acids*, pp 13−25, John Wiley & Sons, Ltd., New York.
27. Roberts, J. D., Yu, C., Flanagan, C., and Birdseye, T. R. (1982) *J. Am. Chem. Soc. 104*, 3945−3949.
28. Wei, Y., de Dios, A. C., and McDermott, A. E. (1999) *J. Am. Chem. Soc. 121*, 10389−94.
29. Mizuguchi, H., Cook, P. F., Tai, C.-H., Hasemann, C. A., and Uyeda, K. (1999) *J. Biol. Chem. 274*, 2166−75.
30. Yuen, M. H., Mizuguchi, H., Lee, Y.-H., Cook, P. F., Uyeda, K., and Hasemann, C. A. (1999) *J. Biol. Chem. 274*, 2176−2184.
31. Pilkis, S. J., Regen, D. M., Stewart, H. B., Pilkis, J., Pate, T. M., and El-Maghrabi, M. R. (1984) *J. Biol. Chem. 259*, 949−58.
32. Stewart, H. B., El-Maghrabi, M. R., and Pilkis, S. J. (1986) *J. Biol. Chem. 261*, 8793−8.
33. Hultquist, D. E., Moyer, R. W., and Boyer, P. D. (1966) *Biochemistry 5*, 322−331.

BI000815K